Small-angle neutron scattering from multilamellar lipid bilayers: Theory, model, and experiment

Lemmich, Jesper; Mortensen, Kell; Ipsen, John Hjorth; Callisen, Thomas Hønger; Bauer, Rogert; Mouritsen, Ole G.

Published in:
Physical Review E. Statistical, Nonlinear, and Soft Matter Physics

Link to article, DOI:
10.1103/PhysRevE.53.5169

Publication date:
1996

Document Version
Publisher's PDF, also known as Version of record

Small-angle neutron scattering from multilamellar lipid bilayers: Theory, model, and experiment

Jesper Lemmich,[1] Kell Mortensen,[2] John Hjort Ipsen,[1] Thomas Hønger,[1] Rogert Bauer,[3] and Ole G. Mouritsen,[1]
[1]*Department of Physical Chemistry, The Technical University of Denmark, Building 206, DK-2800 Lyngby, Denmark*
[2]*Department of Solid State Physics, Risø National Laboratory, DK-4000 Roskilde, Denmark*
[3]*Department of Physics, Royal Veterinary and Agricultural University of Denmark, Thorvaldsensvej 40, DK-1871 Frederiksberg, Denmark*
(Received 31 October 1995)

Small-angle neutron scattering data obtained from fully hydrated, multilamellar phospholipid bilayers with deuterated acyl chains of different length are presented and analyzed within a paracrystalline theory and a geometric model that permit the bilayer structure to be determined under conditions where the lamellar layers are coupled and fluctuating. This theory provides structural information in the region of the solid-fluid bilayer phase transition without invoking the usual decoupling of the scattering intensity function into form and structure factors. Results are presented as a function of temperature for the lamellar repeat distance, the hydrophobic bilayer thickness, as well as the thickness of the aqueous and polar head group region. In addition to these geometric parameters the analysis permits determination of molecular cross-sectional area, number of interlamellar water molecules, as well as estimates for response functions such as lateral area compressibility. The results, which are compared to experimental data obtained by other techniques, provide indirect information on interlamellar undulation forces, renormalization of bilayer bending rigidity, and unbinding phenomena in multilamellar stacks. [S1063-651X(96)05605-X]

PACS number(s): 87.64.Bx, 64.60.Fr

I. INTRODUCTION

The fluid-lipid bilayer component of cell membranes is an ubiquitous structural element of living matter [1]. A structural characterization of this bilayer and a determination of its physical properties are essential for providing a basis for understanding structure-function relationships in biological membranes [2], e.g., regulation of protein and enzyme functions by lipid structure and dynamics. Under most physiological conditions the pseudo-two-dimensional lipid bilayer is in a fluid (liquid) state under excess water conditions and it may exhibit substantial excursions into the third dimension. This implies a high degree of disorder. Still, the bilayer integrity assures a well-defined structural profile in the direction normal to the bilayer surface. Pure lipid bilayers in aqueous suspension are commonly used as models of biological membranes. To facilitate structural studies, the lipid bilayers are usually studied in a multilamellar configuration in which a large number of layers are arranged in a stack in which adjacent bilayers are approximately parallel, with an aqueous layer in between as illustrated in Fig. 1. For noncharged phospholipids in water the assembly into a multilamellar stack with a well-defined and finite repeat distance is a spontaneous process. To ensure maximal interlamellar coherence and effectively flat bilayers the system may be prepared as an oriented sample using an assay with glass plates. A large number of experimental techniques have been used to determine the bilayer structural profile and the hydration properties of model membranes, notably solid-state nuclear magnetic resonance techniques [1], and x-ray and neutron scattering [3–6].

Lipid bilayers exhibit phase transitions [7, 8], one of which is the so-called main phase transition, which takes the bilayer from a low-temperature solid (gel) phase to a high-temperature fluid (liquid-crystalline) phase at a transition temperature T_m whose value depends on the lipid material in question. The transition implies major structural changes within the bilayer. The fluid phase is a liquid (the L_α phase) with both translational disorder as well as a high degree of lipid-acyl-chain disorder. The gel phase is a pseudo-two-dimensional crystalline solid in which the lipid-acyl chains

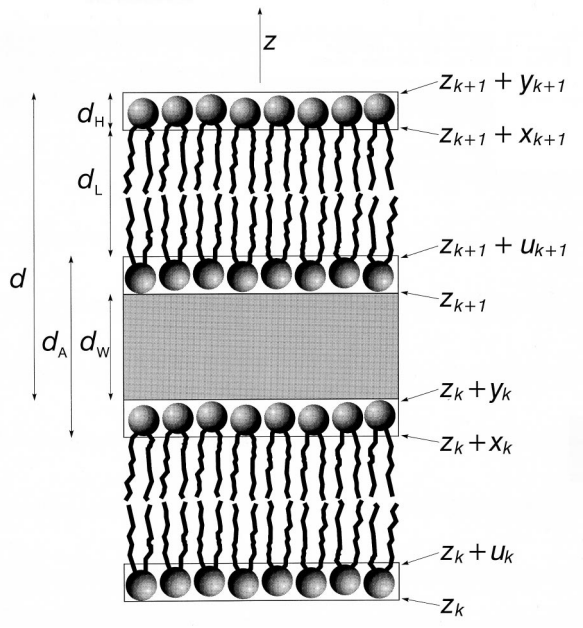

FIG. 1. Schematic illustration of a multilamellar array of lipid bilayers. Lamellar repeat distance is d, hydrophobic lipid bilayer thickness is d_L, and hydrophilic layer thickness is $d_A = d_W + 2d_H$. The coordinates indicated on the left hand side refer to the use in Eqs. (10) and (11).

are conformationally highly ordered. This implies that, as the bilayer is taken through the main transition, its thickness is altered and there is a concomitant change in the bilayer area. The relative change of membrane volume during the transition remains small compared to the relative thickness and area changes [9, 10]. For the type of phospholipids that we are concerned with in the present paper, di-acyl phosphatidylcholines DMPC and DPPC [11], the gel phase immediately below T_m is a rippled ($P_{\beta'}$) phase. At a lower temperature there is yet another transition, the pretransition, that transforms the ripple phase into a planar solid phase, $L_{\beta'}$. We shall not be concerned with this transition in the present paper.

The main transition in multilamellar bilayers of DMPC and DPPC is a first-order phase transition which, however, is close to a critical point [8, 12]. There is both experimental [13] and theoretical [14] evidence that the bilayers with the shorter chain length display stronger critical fluctuations. The proximity to a critical point implies not only strong in-plane bilayer density fluctuations but also out-of-plane undulations due to an effective thermal renormalization of the bilayer bending rigidity [15, 16]. These strong fluctuations have significant implications for the analysis of the scattering data in the transition region, since it means that the form and structure factors of the scattering intensity function can not be decoupled.

In the present work we study multilamellar systems of DMPC and DPPC whose acyl chains are fully deuterated (DMPC-d_{54} and DPPC-d_{62}) at excess water conditions. We have studied nonoriented samples in order to be able to examine the case of an unconstrained system in which the interlamellar forces, within a reasonable equilibration time ($\sim$1/2 hour) and under strongly fluctuating conditions, can fully manifest themselves and lead to thermodynamic swelling equilibrium. The samples are prepared in D_2O. This provides maximal contrast in scattering length density along the bilayer profile, since the head groups have considerably lower scattering length density than D_2O and the deuterated acyl chains. Furthermore, this procedure will ensure that the incoherent scattering, which mainly stems from the large incoherent scattering cross section of the hydrogen atoms, is minimized.

The substantial thermal fluctuations in the multilamellar lipid stack taken together with a lack of true long-range order in the stack imply that we are dealing with both thermal disorder (disorder of first kind), i.e., disorder in which the molecules oscillate around well defined positions, and lattice disorder (disorder of second kind), where a uniform unit cell is lacking [3, 17]. For analyzing the scattering data we have used a version of one-dimensional paracrystalline theory [18] together with a simple strip model in which each of the layers of the lamellar stack is subject to Gaussian fluctuations.

The general aim of the study is to obtain, from a single experiment and with a minimal set of assumptions, structural data for lipid bilayers together with certain physical properties, such as molecular cross-sectional area, number of interlamellar water molecules, as well as estimates for response functions such as lateral area compressibility. With the temperature dependence of these structural and thermomechanic properties available, in particular in the region of the main phase transition, we are in the position to investigate and discuss interesting physical phenomena, such as pseudocritical behavior, anomalous swelling, interlamellar undulation forces, and critical unbinding transitions.

The layout of the paper is as follows. In Sec. II we present a general discussion of scattering from multilamellar lipid bilayers and argue that for the present purpose the paracrystalline theory [18] is more suited to analyze the small-angle neutron-scattering (SANS) data than Caillé theory [19]. The particular version of paracrystalline theory used and the model of the bilayer system invoked to parametrize the theory are presented in Sec. III. In Sec. IV the sample preparation is described together with details of the SANS measurements. General aspects of the data analysis are put forward in Sec. V, and some results hereof are shown in Sec. VI. A comparison with other relevant experimental data for selected properties is given in Sec. VII. The paper is concluded in Sec. VIII.

II. SCATTERING FROM MULTILAMELLAR LIPID BILAYERS

The scattering intensity function $I(q)$ from x-ray and neutron scattering of soft, layered systems can in the Born approximation be interpreted in terms of a form factor $f(q)$ and a structure factor $s(q)$. $f(q)$ characterizes the scattering length density b in a repeat unit, since it is just the Fourier amplitude of b, and $s(q)$ describes the crystalline or quasicrystalline nature of the layered system. The relationship between $I(q)$, $s(q)$, and $f(q)$ is given by

$$I(q)=\langle|f(q)|^2 s(q)\rangle. \tag{1}$$

Here $\langle\ \rangle$ denotes averaging over all fluctuations in the system. The fluctuations of $f(q)$ and $s(q)$ can in most experimental systems be considered as independent, which implies that the form and structure factors can be decoupled according to

$$I(q)=\langle|f(q)|^2\rangle\langle s(q)\rangle. \tag{2}$$

Furthermore, one often neglects the fluctuations of the form factor and writes

$$I(q)=\langle|f(q)|\rangle^2\langle s(q)\rangle=|F(q)|^2 S(q). \tag{3}$$

The last step can be justified in cases where one is probing the q regions in the immediate vicinity of the Bragg peaks only (as is the case within Caillé theory as described below). In those cases the fluctuations in the form factor are expected to give rise only to diffuse background scattering [20].

The structure factor of soft layered systems has previously been described in terms of Caillé theory [19]. Caillé theory accounts for the elastic deformations of the layer positions. In the standard continuum formulation of Caillé theory, the free-energy density g is given by a harmonic expression

$$g=\frac{K}{2}\left(\frac{\partial^2 u}{\partial x^2}+\frac{\partial^2 u}{\partial y^2}\right)^2+\frac{B}{2}\left(\frac{\partial u}{\partial z}\right)^2, \tag{4}$$

where $u(x,y,z)$ is the local displacement of the layers along the z direction normal to the layers [21]. K is the layer bending modulus and B is the bulk modulus of layer compres-

sion. It was demonstrated by Caillé that the contribution from Eq. (3) to the scattering intensity close to the nth order Bragg peak in the z direction of oriented layers takes the form [19]

$$S(0,0,q_z) \propto \left(q_z - n\frac{2\pi}{d} \right)^{-2+\eta_n}, \tag{5}$$

where

$$\eta_n = \frac{\pi}{2d^2} \frac{k_B T}{\sqrt{KB}} n^2 \tag{6}$$

and d is the repeat distance. Taking the thickness δ of the layers into account, important finite-size corrections appear [22, 23]:

$$\eta_{n,\delta/d} = \eta_n (1-\delta/d)^2. \tag{7}$$

This general behavior was experimentally confirmed by Als-Nielsen *et al.* [24] for smectic-*A* liquid crystalline systems and by Safinya *et al.* [23] for the diluted limit of a microemulsion L_α phase. The description of the structure factor of soft, layered systems in terms of Caillé theory has therefore become an important tool for gaining information about the elastic constants from the scattering profiles around the Bragg positions [25].

In the present work we have chosen not to use Caillé theory to analyze and interpret the scattering data from the lamellar phases of DMPC-d_{54} and DPPC-d_{62} close to the main phase transitions. There are several reasons for this.

We do not expect that the simple decoupling of the form and structure factors according to Eq. (2) and (3) is appropriate for bounded membranes close to the main phase transition, since significant changes in the structure of the membranes (e.g., bilayer thickness) and the intermembrane distances take place concomitantly at comparable length scales. Further, strong fluctuations are expected near the main phase transition both in the membrane thickness and in the interlamellar spacings. We have no reason to expect that these fluctuations are uncoupled, which could justify the decoupling of the form and structure factors in the scattering intensity function. Finally, we do not expect the simple harmonic theory of the fluctuations in the positions of the lamellae, which is the basis of Caillé theory [19], to be a good starting point for the description of the structure of the system close to the main phase transition. The strong in-plane density fluctuations couple to the membrane mean curvature and at distances that are large compared to the in-plane correlation length this coupling gives rise to an effectively decreased bending modulus due to thermal roughening of the membrane at shorter length scales [15]. A substantial reduction of the bending rigidity for both DMPC and DPPC in unilamellar vesicles has been demonstrated recently experimentally by flicker-noise analysis [26]. At length scales at the order of nanometers the renormalization of the bending modulus is, however, a more subtle problem, and the description of Eq. (4) becomes insufficient in describing even the low-energy fluctuations in the system. Yet another problem in interpreting scattering data on the basis of the harmonic theory in Eq. (4) arises as we approach the critical unbinding point of membranes [27–29] where the elastic modes in the system get strongly correlated and the interpretation of the Bragg-peak profiles in terms of elastic moduli of the layered system becomes obscure. In light of these considerations, it does not seem within reach to put forward a Hamiltonian theory that accurately describes the physics of the layered lipid system close to the main phase transition.

Our modeling of the scattering intensity aims primarily at getting accurate geometrical information about the layered lipid bilayer system from the full scattering intensity up to the third order Bragg peak, while we do not attempt to address the question about the nature of the one-dimensional crystallinity directly from, e.g., analyses of line-shape profiles as has been done on x-ray scattering data [30, 31]. The geometrical information is obtained via a parametrization of the theory in terms of a simple model. This model complies with the demand that the coupling between the form and structure factors is explicitly accounted for by statistically describing the actual spatial extension of the lipid bilayers and the aqueous layers in between.

The basis of the theory is the paracrystalline theory of Hosemann and Baggchi [18]. It is a purely geometric one-dimensional theory, which provides structural information on the layered system from the entire scattering intensity function. By restricting ourselves to a one-dimensional model (a strip model), the fluctuations in the system are accounted for in an averaged way.

As argued above, we shall for theoretical reasons use the paracrystalline theory rather than Caillé theory to analyze our experimental data. However, we have performed a parallel analysis [32] in terms of the Caillé theory and found, as expected, that whereas the paracrystalline theory is superior in the $P_{\beta'}$ phase and in the transition region, the experimental data in the fluid phase are equally well described by the two theories.

The actual way to adapt the paracrystalline theory to the layered lipid bilayer system and how the theory is parametrized will be described in the next section.

III. MODEL AND PARACRYSTALLINE THEORY

In this section we will derive an expression for the expectation value of the intensity function for scattering by a multilamellar array of fully hydrated lipid bilayers, using a version of paracrystalline theory [18, 33] that is parametrized in terms of a simple strip model, cf. Fig. 1. The theory enables us to perform a fit to the experimental data and thereby to obtain information about the structural amplitudes along the bilayer profile. Once these are obtained we shall show that it is straightforward to derive other properties, such as molecular cross-sectional area and volumetric properties as well as the associated standard deviations, which can be related to thermal response functions, such as lateral area compressibility.

Under the assumption that the radii of curvature of the multilamellar vesicles are large compared to the thickness of the individual bilayers, the system can be described as consisting of stacks of N nearly flat bilayers. Within this description the scattering intensity function $I(q)$ is given by

$$I(q) = \frac{I_1(q)}{q^2} = \frac{\langle |f(q)|^2 s_1(q) \rangle}{q^2}, \tag{8}$$

where q^{-2} is the Lorentz factor for nonoriented powder samples [30] and $I_1(q)$ is the one-dimensional intensity function calculated along the direction $\vec{z}$ normal to the plane of the lamellae (i.e., $q_z \rightarrow q$); cf. Fig. 1. $s_1(q)$ is the corresponding one-dimensional structure factor.

In order to parametrize the theory for $I_1(q)$ we apply a simple geometric model in which each of the N repeat units in a stack is taken to consist of four layers with different scattering length densities; b_H (for the two head-group regions), b_W (for the water layer), and b_L (for the hydrophobic acyl-chain layer), as illustrated in Fig. 1. The acyl chains are fully deuterated. Since the scattering lengths for deuterium, carbon, and oxygen are comparable in size and considerably larger than that for hydrogen [34], we have included the acyl-oxy groups in the definition of the hydrophobic layer. The thickness of the layers is assumed to fluctuate independently according to Gaussian distributions with mean values d_H, d_W, and d_L, and corresponding standard deviations σ_H, σ_W, and σ_L. According to the Babinet principle, the neutron scattering length density of the solvent b_W can be chosen as a reference, implying that b_H and b_L are evaluated relative to b_W, i.e.,

$$\tilde{b}_H = \overline{b_H} - \overline{b_W}, \quad \tilde{b}_L = \overline{b_L} - \overline{b_W}. \tag{9}$$

We are now in a position to derive an expression for $I_1(q)$. The expression is in principle just an extension of the one derived in Ref. [18] from two to four independently varying layers. In terms of the form factor for the kth layer (cf. Fig. 1)

$$\begin{aligned} f_k(q) &= \int_{\text{repeat unit}} \tilde{b}(z) e^{-iqz} dz \\ &= \int_{z_k}^{z_k+u_k} \tilde{b}_H e^{-iqz} dz + \int_{z_k+u_k}^{z_k+x_k} \tilde{b}_L e^{-iqz} dz \\ &\quad + \int_{z_k+x_k}^{z_k+y_k} \tilde{b}_H e^{-iqz} dz \\ &= \frac{1}{iq}[\tilde{b}_H(1-e^{-iqy_k}) + (\tilde{b}_L - \tilde{b}_H)(e^{-iqu_k} - e^{-iqx_k})], \end{aligned} \tag{10}$$

the total amplitude of the one-dimensional intensity function is given by

$$\begin{aligned} I_1(q) &= \left\langle \sum_{j=1}^{N} \sum_{k=1}^{N} f_j(q) f_k^*(q) e^{-iq(z_j - z_k)} \right\rangle \\ &= \left\langle |f(q)|^2 \left(N + 2 \sum_{k=1}^{N-1} (N-k) e^{-iqz_k} \right) \right\rangle \\ &= \langle |f(q)|^2 s_1(q) \rangle, \end{aligned} \tag{11}$$

where we have used that the form factors for the individual layers are statistically independent and the layer index k therefore can be omitted. Some authors prefer at this point to separate the scattering intensity function into an average form factor and an average structure factor corresponding to Eq. (2) (lattice model), instead of performing the average on the product (stacking model) [35–37]. In light of the discussion presented in Sec. II, it is important to emphasize that in the present work we have not separated the form and structure factors in the averaging procedure but averaged the product directly. In this sense our use of the term paracrystalline theory corresponds to that of the classical work of Ref. [18] but is fundamentally different from the way the term has been used recently, e.g., by Nagle and collaborators [38] who use it in connection with the decoupling scheme $\langle |f(q)|^2 s_1(q) \rangle \rightarrow \langle |f(q)|^2 \rangle \langle s_1(q) \rangle \rightarrow |\langle f(q) \rangle|^2 \langle s_1(q) \rangle$ as in Eq. (3). This type of decoupling assumes that the fluctuations in the bilayer thickness are negligible and there is only a substantial fluctuation in the layer periodicity.

By introducing the Fourier transform of the Gaussian distribution functions

$$F_\nu(q) = e^{-iqd_\nu - (1/2)q^2\sigma_\nu^2}, \tag{12}$$

with $\nu = H, L, W, D$ (where $d_D = d$) we obtain after some algebra

$$I_1(q) = \frac{2N\tilde{b}_H^2}{q^2} \left[i_B(q) + \frac{1}{N} i_C(q) \right] \tag{13}$$

with

$$i_B(q) = \mathrm{Re}\left[\frac{(1-F_W)(1-F_H^2F_L) + (\tilde{b}_r - 1)^2(1-F_L)(1-F_H^2F_W)}{1-F_D} \right] + \mathrm{Re}\left[\frac{2(\tilde{b}_r - 1)F_H(1-F_W)(1-F_L)}{1-F_D} \right], \tag{14}$$

$$i_C(q) = \mathrm{Re}\left[F_W(1-F_D^N) \left(\frac{(1-F_H^2F_L) + (\tilde{b}_r - 1)F_H(1-F_L)}{1-F_D} \right)^2 \right], \tag{15}$$

where

$$\tilde{b}_r = \frac{\tilde{b}_L}{\tilde{b}_H} \tag{16}$$

and

$$F_D = F_H^2 F_L F_W. \tag{17}$$

Re denotes the real value of the function. Since $I(q) \propto q^{-2} I_1(q)$ we obtain

$$I(q) = \frac{\Gamma}{q^4} \left[i_B(q) + \frac{1}{N} i_C(q) \right], \tag{18}$$

where Γ is a normalization constant. In the high-q limit we get the asymptotic form

$$I_\infty(q)=\frac{\Gamma}{q^4}[1+(\tilde{b}_r-1)^2]. \tag{19}$$

When $\tilde{b}_r$ and the distribution functions of the individual layers are known, we can calculate the molecular cross-sectional area A since by definition

$$\tilde{b}_H=\frac{\Sigma_{i,H}b_i}{d_H A}, \quad \overline{b_L}=\frac{\Sigma_{i,L}b_i}{d_L A}. \tag{20}$$

In these expressions, the average scattering length density of a given group of atoms is derived by summing up the individual scattering lengths of the atoms involved and then dividing by the volume, which to first order is given as above (i.e., we neglect higher order correlations). By assuming a temperature-independent water density, $\rho_{\mathrm{D_2O}}$, $\overline{b_W}$ can be calculated from

$$\overline{b_W}=\frac{N_A\rho_{\mathrm{D_2O}}\Sigma_{i,\mathrm{D_2O}}b_i}{M_{\mathrm{D_2O}}}. \tag{21}$$

Using these expressions for the average scattering-length densities, Eqs. (20) and (21), we obtain

$$A=\left(\frac{\sum_{i,L} b_i}{\overline{b_W}(1-\tilde{b}_r)}\right)\frac{1}{d_L}-\left(\frac{\tilde{b}_r\sum_{i,H} b_i}{\overline{b_W}(1-\tilde{b}_r)}\right)\frac{1}{d_H} \tag{22}$$

$$=\frac{\alpha}{d_L}+\frac{\beta}{d_H}. \tag{23}$$

With $\rho_{\mathrm{D_2O}}=1100\ \mathrm{kg\,m^{-3}}$, $N_A=6.024\times10^{23}\ \mathrm{mol^{-1}}$, and $M_{\mathrm{D_2O}}=0.020\ \mathrm{kg\,mol^{-1}}$ together with the values for b_i given in Ref. [34] we find

$$\alpha_{\text{DMPC-}d_{54}}=\frac{1796.6\ \text{Å}^3}{1-\tilde{b}_r}, \quad \alpha_{\text{DPPC-}d_{62}}=\frac{2048.9\ \text{Å}^3}{1-\tilde{b}_r},$$

$$\beta=-\tilde{b}_r\frac{31.17\ \text{Å}^3}{1-\tilde{b}_r}, \tag{24}$$

where it is understood that the lipid-acyl chains are fully deuterated.

By a similar procedure, volumetric properties such as molecular lipid volume and total volume per molecule can be derived to first order. One quantity of particularly interest is the number of water molecules per lipid molecule, which to first order is given by

$$n_W=\frac{N_A\rho_{\mathrm{D_2O}}}{M_{\mathrm{D_2O}}}\frac{d_W A}{2}. \tag{25}$$

Neglecting higher order correlations in the derivation of A and the volumetric quantities corresponds in reality to assuming that these quantities do not fluctuate. It is, however, possible to derive Gaussian fluctuations in A and the volumetric quantities to first order in σ_L, σ_H, and σ_W, again by neglecting higher order correlations. As an example, we get, from Eq. (23), to first order

$$\sigma_A=\sqrt{\left(\frac{\alpha\sigma_L}{d_L^2}\right)^2+\left(\frac{\beta\sigma_H}{d_H^2}\right)^2}. \tag{26}$$

The isothermal lateral area compressibility κ_A is defined by the fluctuation-dissipation relation

$$\kappa_A=\frac{1}{k_B T}\frac{\langle A^2\rangle_T-\langle A\rangle_T^2}{\langle A\rangle_T}, \tag{27}$$

where $\langle\ \rangle_T$ denotes the true thermal average. For comparison we define

$$\tilde{\kappa}_A=\frac{1}{k_B T}\frac{\sigma_A^2}{A} \tag{28}$$

and use this quantity as an estimate for the lateral area compressibility. We do not contend that this kind of estimate, derived from Gaussian thickness fluctuations, provides an adequate way of measuring the lateral area compressibility, but a comparison between $\tilde{\kappa}_A$ and experimentally obtained values of κ_A is useful, since it gives us an opportunity to evaluate to which extent the Gaussian fluctuations derived from our model represent the thermal fluctuations in the system.

It should be emphasized that in the above model, we assume that the head group region and the water region are clearly separable. Obviously this is an oversimplification relative to the real system, since we are then neglecting the fact that the hydration of the head group will tend to smooth out the boundary between the two regions. When we present the results for the geometric parameters obtained, we shall therefore refer to the total hydrophilic layer thickness, $d_A=2d_H+d_W$ (cf. Fig. 1). It becomes more subtle when we turn to the molecular cross-sectional area. It is probably a good approximation to assume that the region, specified by d_W, has the same density as the bulk water [cf. Eq. (21)]. The main problem is that the head group region has a larger scattering length density than indicated, since it also contains an unknown amount of water molecules. This implies that the numerical value of β is systematically underestimated. However, since the experiments have been designed so that $\tilde{b}_r$ is small ($\overline{b_L}\simeq\overline{b_W}>\overline{b_H}$), β will in any case be very small compared to α. Thus, the effect on the estimate for A of neglecting the hydration of the head groups is expected to be small.

The above considerations suggest that if we compare our definitions with the formalism developed by Nagle and Wiener [39], the value n_W, as defined above, corresponds to n_W-n_W' in their definition. They define n_W as the total number of water molecules per lipid molecule between the bilayers, whereas n_W' is defined as the number of water molecules per lipid between head groups in the same monolayer.

Another issue that deserves some discussion is how well we can expect the model to describe the system in the $P_{\beta'}$ phase, where the ripples are known to give rise to additional scattering peaks as first described by Tardieu, Luzatti, and Reman [40]. First of all one observes a (0,1) peak character-

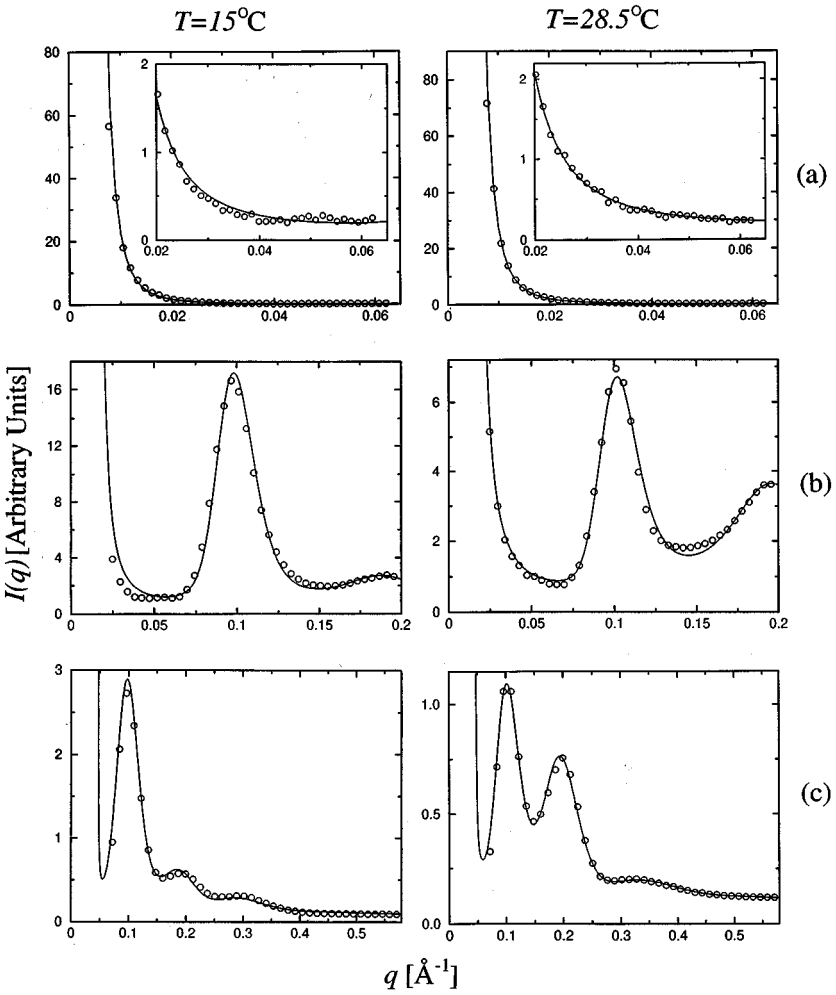

FIG. 2. Experimentally obtained scattering functions (○) (smeared data) and fits for DMPC-d_{54} at $T=15$ °C and $T=28.5$ °C. (a) Type-II fits (low-q spectra). The inserts are magnifications of parts of the spectra. (b), (c) Type-I fits to the intermediate-q and high-q spectra, respectively.

izing the ripple repeat distance, but also higher order peaks, such as (0,2), (1,1), and (2,1), which will appear as ''shoulders'' on the main Bragg peaks. The intensity of these additional peaks is quite pronounced when the water content is low [41–43]. In nonoriented multilamellar systems under excess water conditions, the peaks become less pronounced, but the (0,1) and the $(n,1)$ peaks can still be detected if the resolution is good enough [44–46]. We shall return to this point in Sec. V.

IV. MATERIALS AND EXPERIMENTAL METHODS

DMPC and DPPC with perdeuterated fatty acid chains (DMPC-d_{54} and DPPC-d_{62}) were obtained from Avanti Polar Lipids Inc. (Birmingham, AL). The materials were used without further purification.

The samples were prepared by dissolving 110 mg lipid in $CHCl_3$. The solvent was subsequently evaporated under dry nitrogen atmosphere and further dried under vacuum in order to remove traces of the solvent. Multilamellar bilayers were formed by hydrating the dry lipid in 0.5 ml D_2O buffer [50 mM Hepes $\sim p$D 7.2, 10 mM NaCl, 1 mM NaN_3, and 60 μM ethylenediamine tetra-acetic acid (EDTA)] at $T=T_m+10$ °C. Two samples were prepared independently for each of the two lipids. It is important in order to observe the equilibrium swelling behavior in the transition region that the lipid dispersion contains sufficient water (excess water) to provide full hydration. In the present case we have used samples with approximately 85 wt. % water. The samples were temperature cycled through T_m and vortex mixed numerous times throughout a 2-hour hydration period. The equilibrium phase behavior of the samples was checked by differential-scanning calorimetry (Microcal MC-2).

The samples were mounted in a sealed quartz container (Suprasil from Hellma, Germany) with 2-mm flight path. The SANS scattering experiments were performed using the Risø-SANS facility. To obtain the neutron spectra of pure water, used for calibration, a 1-mm-thick quartz container was used. The samples were investigated under three different experimental conditions. 2.8-Å neutrons were used with sample-to-detector distances of 1 and 3 m, corresponding to scattering vectors in the high-q range 0.07–0.58 $Å^{-1}$ and the intermediate-q range 0.02–0.2 $Å^{-1}$, respectively. 9-Å neutrons were used with a sample-to-detector distance of 3 m in order to cover the low-q range 0.007–0.06 $Å^{-1}$. The neutron wavelength resolution was $\Delta\lambda/\lambda=0.18$, and the neutron beam collimation was determined by the pinhole sizes of 16- and 7-mm diameter at source and sample position, respectively. The scattering data were corrected for background arising from the quartz container with D_2O and from other sources, as measured with the neutron beam blocked by plastic-containing boron at the sample position. The incoherent scattering from H_2O was used to take the

deviation from a uniform detector response into account. The scattering patterns were all azimuthally isotropic. The data were therefore circularly averaged into one-dimensional intensity functions $I(q)$, only dependent on the absolute value of the wave vector q.

A series of experiments was performed at all three settings in the temperature ranges $T=12-32\,^{\circ}\mathrm{C}$ for DMPC-d_{54} and $T=31-49^{\circ}\mathrm{C}$ for DPPC-d_{62}. In all cases the samples were heated stepwise allowing for an equilibration time of 30 min at each temperature step.

V. DATA ANALYSIS

In this section we will describe how the model and the paracrystalline theory put forward in Sec. III are used for analyzing the experimental scattering data. Details of some of the results obtained by the analysis are given in Sec. VI.

Representative examples of the scattering data for the different q ranges are shown in Fig. 2 in the case of DMPC-d_{54} at $T=15\,^{\circ}\mathrm{C}$ and 28.5°, corresponding to the $P_{\beta'}$ phase and the L_{α} phase, respectively (as confirmed by differential-scanning calorimetry). The fact that the structural states of the lipid bilayer and the multilamellar array are quite different in the two phases clearly manifests itself in the form of the scattering function. Three orders of Bragg reflections, (1,0), (2,0), and (3,0), can be discerned. The higher the order of the reflection, the broader it is. This observation also holds true when instrumental smearing is taken into account and it indicates that the lamellar stack displays disorder of the second kind [3]. At $T=15\,^{\circ}\mathrm{C}$ the (0,1) reflection of the ripples appears as a very broad peak between $q\simeq 0.04$ and 0.06 $\mathrm{\AA}^{-1}$ [cf. the inset of Fig. 2(a)]. Although weak in amplitude, this peak is clearly visible for all temperatures below T_m. The position of the peaks is in good agreement with the observations of Matuoka *et al.* [44]. No higher order peaks characterizing the ripples can be detected. It should be noted that $I(q)$ in Fig. 2 is displayed in arbitrary units. The analysis of the data, described below, was performed using a nonlinear least-squares fitting routine. The smearing induced by the different instrumental procedures is taken into account in the data analysis as described elsewhere [47].

We performed fits of the theoretical expression, Eq. (18), simultaneously to both the intermediate-q spectrum and the high-q spectrum. In order to perform such a fit, one needs 11 free parameters, i.e., $\tilde{b}_r$, N, d_L, d_H, d_W, σ_L, σ_H, σ_W, and Γ, together with a scale factor that accounts for the relative intensity difference between the two spectra as well as the incoherent background I_{inc} arising from the sample.

Preliminary analysis also showed that I_{inc} couples strongly to the other parameters, thus making the fits unstable. Therefore, it was decided to estimate I_{inc} beforehand. Assuming that the tails of the high-q spectrum can be adequately described by the asymptotic form, Eq. (19), I_{inc} can be determined as the slope of a plot of $I(q)q^4$ versus q^4 [35] as shown in Fig. 3.

The preliminary analysis showed that σ_H is very small. In fact, a precise fit to σ_H is not possible within the resolution of the present type of experiment. Consequently, σ_H was fixed to be zero. It should be noted that in this limit, some oscillations are introduced in Eq. (17). Nevertheless, these oscillations do not affect the conclusions regarding I_{inc}.

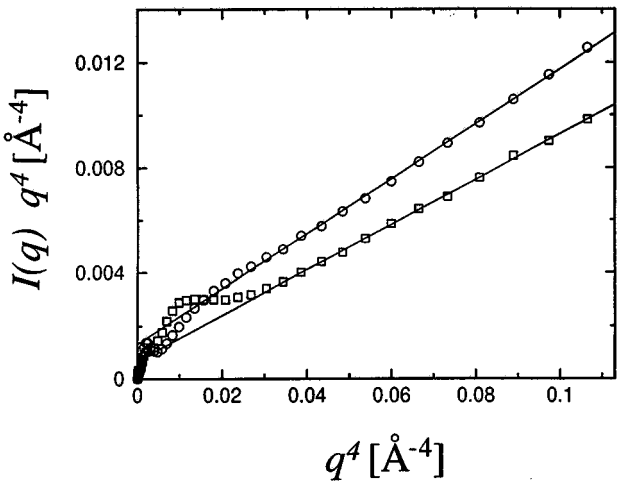

FIG. 3. Plot of $I(q)q^4$ vs q^4, from which the incoherent background scattering I_{inc} can be determined as the asymptotic slope. □: DMPC-d_{54} at $T=15\,^{\circ}\mathrm{C}$; $I_{\mathrm{inc}}=0.0861\pm0.0007$ (fit to the 12 data points at highest q). ○: DMPC-d_{54} at $T=28.5\,^{\circ}\mathrm{C}$; $I_{\mathrm{inc}}=0.1026\pm0.0010$ (fit to the 14 data points at highest q). The instrumental smearing was taken into account in the linear fits.

Furthermore, it was assumed initially that the number of correlated layers, N, is large enough in order for the contribution from $i_C(q)$ in Eq. (16) to be negligible, i.e., $i_B(q)\gg(1/N)i_C(q)$ in the relevant q range. The number of free parameters is thus reduced to 8, and good fits (denoted type I) were obtained in all cases.

In order to estimate N, the number of layers, the low-q spectra were fitted to the full expression, Eq. (16), under the constraint that all structural parameters were fixed to the values obtained from the type-I fit. Thus only two free parameters were needed, i.e., N and a scale factor. However, one problem arises from this procedure. The factor F_D^N in $i_C(q)$ introduces short-wavelength oscillations in the low-q region. These oscillations are not observed experimentally, since they stem from the fact that all multilamellar stacks are assumed to have the same size within the theory. If it is assumed that the stack size follows a Gaussian distribution, it is straightforward to show that unless the distribution is very sharp (which is not expected to be the case here), the oscillations will be damped out exponentially when the average over the distribution is performed. Thus it was decided to put F_D^N to zero from the start. Within this approach equally good fits (denoted type II) were obtained with a mean value of N as a result.

Subsequently, type I fits were performed with the value determined for N. Since inclusion of the finite stack size changed the structural parameters up to about 10% in some cases, alternating fits between type-I and type-II fits were performed until consistency was reached.

Examples of the resulting fits to the experimental data are shown in Fig. 2. Some of the structural parameters that arise from these fits and the theoretical expressions in Sec. III are displayed in Table I.

As quoted in Sec. III, the scattering peaks due to the ripples are not taken into account in the analysis of the scattering data in the $P_{\beta'}$ phase. The presence of the broad low-amplitude (0,1) peaks in the low-q spectra is not expected to

TABLE I. Data for DMPC-d_{54} including statistical errors, as obtained from the scattering functions shown in Fig. 2.

	$T=15$ °C	$T=28.5$ °C
d_H (Å)	7.2±0.4	6.4±0.2
d_L (Å)	32.1±0.4	27.9±0.2
d_W (Å)	17.0±0.6	21.1±0.4
σ_H (Å)	0 (fixed)	0 (fixed)
σ_L (Å)	4.2±0.2	3.5±0.1
σ_W (Å)	5.7±0.2	6.2±0.1
A (Å^2)	47.0±0.9	55.8±0.6
σ_A (Å^2)	6.1±0.4	6.9±0.3
n_W	13.2±0.5	19.6±0.4
N	18.7±1.2	32.0±1.1

affect the type-II fits significantly. As for the higher-order reflections, they are not directly visible from the spectra due to the limited resolution, but they will still contribute to the scattering, thus affecting the type-I fits. At first, this means that an nth order Bragg peak $(n,0)$ is artificially broadened and shifted up in q value, since it will also contain the $(n,1)$ peak.

From Ref. [44] we expect this effect to be negligible for the (1,0) peak, since the intensity of the (1,1) peak relative to that of the (1,0) peak is very small, whereas the effect is stronger, regarding the (2,0) peak. Here the two peaks seem to be comparable in size.

The overall effect of this can be revealed by a close inspection of the fits in Fig. 2. One sees that the fit to the (2,0) peak is shifted down in q value with respect to the experimental data in the $P_{\beta'}$ phase, whereas this is not the case in the L_α phase. The fits to the (1,0) peaks are equally good in both cases. Thus the presence of the ripples does not affect the position of the Bragg peaks, but the artificial broadening of the peaks will mean, all other things being equal, that the fluctuations in the system are somewhat overestimated and the quality of the fit is lowered.

Table I shows that the estimate for σ_L is larger in the $P_{\beta'}$ phase than in the L_α phase for DMPC-d_{54}. This is clearly contrary to our expectation, since the acyl chains are expected to be more stiff in the $P_{\beta'}$ phase than in the L_α phase as also measured micromechanically on giant bilayer vesicles [48]. In light of the above considerations this implies that the main effect of neglecting the ripples in the data analysis is that σ_L becomes overestimated in the $P_{\beta'}$ phase. This seems reasonable, since in terms of our simple one-dimensional model, the ripples could be perceived as excess fluctuations in the bilayer thickness. As expected, the quality of the fits (judged by the χ^2 values) was systematically better in the L_α phase than in the $P_{\beta'}$ phase.

In conclusion, because of the presence of the ripples in the $P_{\beta'}$ phase, one should not insist on any too specific physical interpretation of σ_L and values derived from σ_L (i.e., σ_A in Table I) below T_m.

VI. RESULTS FOR d, d_L, d_A, A, AND σ_A

In Figs. 4 and 5 we show a selection of data obtained from the SANS data for both DMPC-d_{54} and DPPC-d_{62} in the full temperature range investigated. These figures contain information on both the behavior in the transition region as well as inside the solid and fluid phases. All data sets clearly expose the respective transition point.

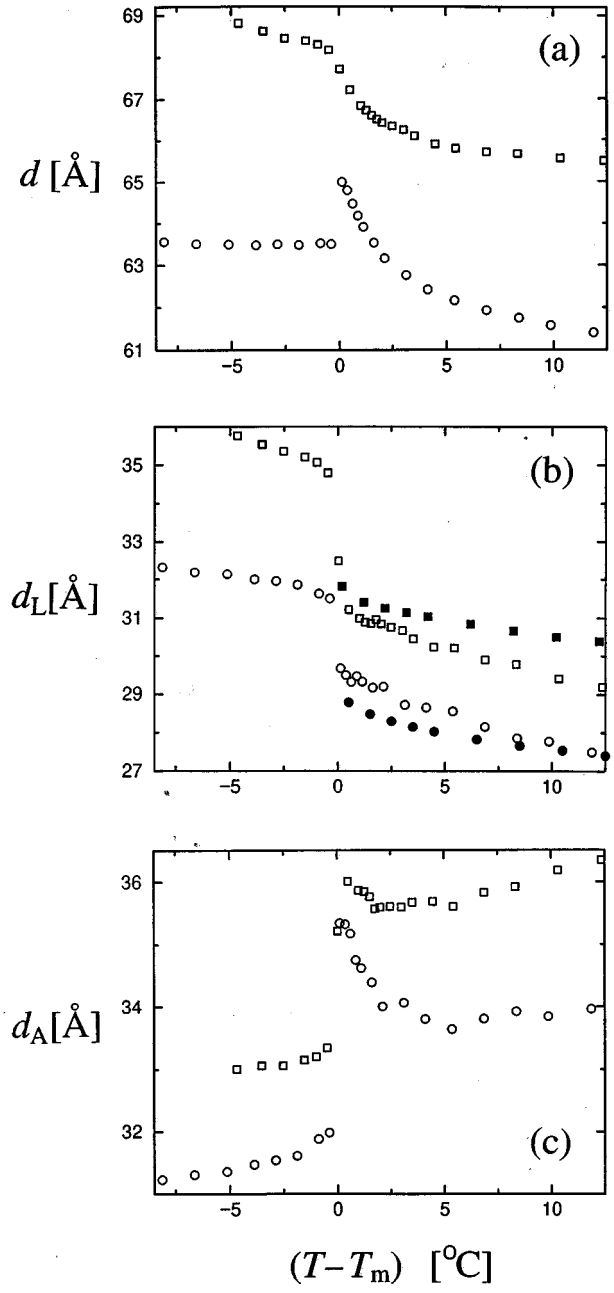

FIG. 4. Lamellar repeat distance d (a), hydrophobic lipid bilayer thickness d_L (b), and hydrophilic layer thickness $d_A=d_W+2d_H$ (c), as functions of reduced temperature, $T-T_m$, for multilamellar bilayers of DMPC-d_{54} (○) and DPPC-d_{62} (□). T_m is the main phase transition temperature. In (b) results are shown as obtained from both SANS measurements (open symbols) and deuterium-NMR measurements (solid symbols) in the fluid phase [13].

The data for the lamellar repeat distance $d(T)$ in Fig. 4(a) show that whereas d only varies little with temperature below T_m there is a rapid decrease above T_m. This behavior is most pronounced for DMPC-d_{54}, which develops a peak in the repeat distance at T_m. The data in Fig. 4(c) demonstrate that the hydrophilic layer thickness d_A is the main source for

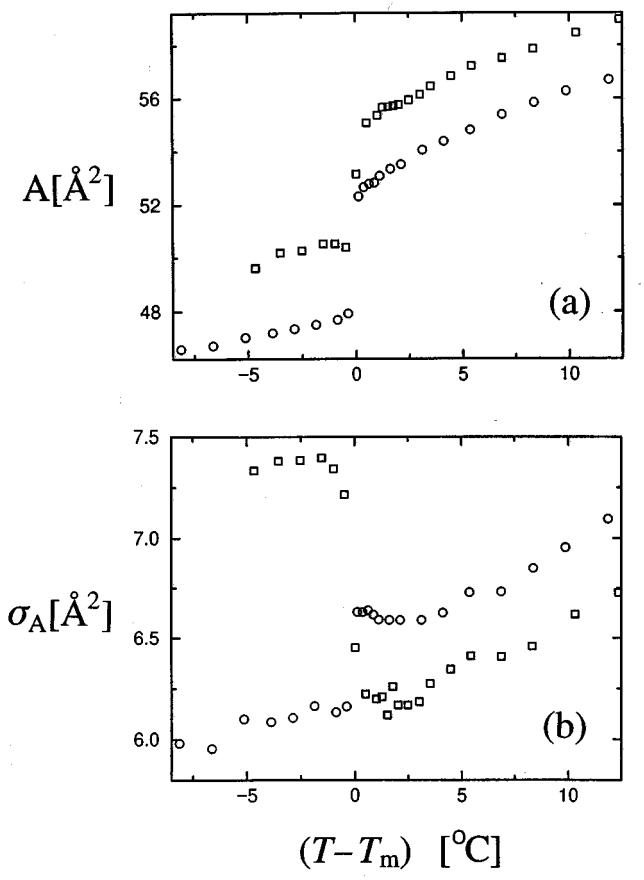

FIG. 5. Molecular cross-sectional area A (a) and corresponding standard deviation σ_A (b) cf. Eq. (25), as functions of reduced temperature, $T-T_m$, for multilamellar bilayers of DMPC-d_{54} (○) and DPPC-d_{62} (□). T_m is the main phase transition temperature.

this anomaly. Even in the case of DPPC-d_{62} d_A displays a peak, which, however, cannot establish its effect in d because the corresponding variation in the hydrophobic thickness d_L is very strong for DPPC-d_{62} as seen in Fig. 4(b). For both DMPC-d_{54} and DPPC-d_{62}, d_L varies monotonously through the transition region. At T_m there is an effective jump corresponding to $\Delta d_L \simeq 2$ Å for DMPC-d_{54} and 4 Å for DPPC-d_{62}.

In Fig. 5 are shown the results for the molecular cross-sectional area A and the corresponding standard deviation σ_A. The area varies strongly in the transition region corresponding to a discontinuity of $\Delta A \simeq 5$ Å^2 for both DMPC-d_{54} and DPPC-d_{62}. The value of A is systematically about 2–3 Å^2 smaller for DMPC-d_{54} than DPPC-d_{62} for all temperatures studied. σ_A is larger for DPPC-d_{62} below the transition whereas the opposite is the case above the transition, but as pointed out in Sec. V, the physical interpretation of the results for σ_A in the $P_{\beta'}$ phase is obscured by the presence of the ripples.

VII. COMPARISON WITH OTHER EXPERIMENTAL DATA

We shall here make a partial comparison of some of the results presented in this paper with selected experimental data obtained by other techniques. This comparison is made in order to illustrate the potential of the present approach. A more complete comparison with other relevant experimental data will be published elsewhere [32].

The results for the repeat distance d in Fig. 4(a) compares favorably with previously published data from small-angle x-ray [31, 42, 49], as well SANS measurements [15] taking into account the well-known fact that different sample preparations lead to slightly different results. In particular the height of the swelling peak at the transition point of DMPC-d_{54} is very sensitive to sample preparation and equilibration procedures [46].

It was originally proposed by Seelig and collaborators [50] that the hydrophobic bilayer thickness d_L could be obtained indirectly from solid-state deuterium-NMR spectroscopy provided that the conformational and rotational motions of the acyl chains are of axial symmetry around the bilayer normal. This is the case in the fluid phase, and it was proposed that there exists a simple approximate linear relationship between the average segmental C-D NMR order parameter, $S_{C\text{-}D}$, and d_L, i.e.,

$$d_L = aS_{C\text{-}D} + b, \tag{29}$$

where a and b are geometric constants. Since $S_{C\text{-}D}$ is easy to measure accurately by standard deuterium nuclear quadrupolar resonance spectroscopy, the hydrophobic bilayer thicknesses can readily be estimated under varying circumstances without performing scattering experiments [52]. The relationship is, however, an approximation and it may not always be reliable as pointed out by Nagle [53]. We can use the present data set in Fig. 4(b) to examine the validity of the relationship for DMPC-d_{54} and DPPC-d_{62}. To this end we use the NMR results obtained by Morrow, Whitehead, and Lu [13]. Since we have included the acyl-oxy group in the definition of d_L used in the present paper, whereas in the NMR measurements this part is not included, we have added 2×3 Å to the NMR results, corresponding to 3 Å per acyl-oxy group. This comparison shown in Fig. 4(b) indicates that the two different types of measurements agree reasonably well within $0.5-1$ Å for both DMPC-d_{54} and DPPC-d_{62}. Therefore the approximation in Eq. (29) can conveniently be used for hydrophobic thickness determination of fluid bilayers in the present case. The same type of comparison cannot be made in the solid $P_{\beta'}$ phase since in this phase the lipid-acyl chains are not oriented normal to the bilayer plane that is required for Eq. (29) to hold.

The molecular cross-sectional areas in Fig. 5(a) are not readily measurable directly by other methods. The conventional way to obtain A proceeds via a method proposed by Luzatti and co-workers [40], which involves weighing out known amounts of water and lipid and requires information about the molar specific volume of the lipid. Similarly, knowledge of lipid chain volumes, V_L, can obviously, together with NMR measurements and Eq. (29), be used to determine A [51]. Nagle [53] has recently, in an attempt to resolve the considerable scatter in the values reported for A from NMR data, estimated A for DPPC-d_{62} to be $A = 62 \pm 2$ Å^2 at 50 °C. Considering the scatter mentioned above, this is quite close to the value that can be read off from the SANS data in Fig. 5(a), $A \simeq 59$ Å^2 at 49 °C, which does not require any prior knowledge of any partial volumes

TABLE II. Thermal area expansivity C_T and estimate for the lateral area compressibility $\tilde{\kappa}_A$ for DMPC-d_{54}, together with C_T and κ_A for DMPC from Ref. [54].

phase	$(T-T_m)$ (°C)	C_T ($°C^{-1}$)	C_T (Ref. [54])	$\tilde{\kappa}_A$ (cm/dyn)	κ_A (Ref. [54])
$P_{\beta'}$	−8	0.0032	0.0058	0.0019	0.016
L_α	5	0.0067	0.0068	0.0020	0.0069
L_α	11	0.0043	0.0042	0.0021	

of the system. From the value of A, Nagle furthermore gives an estimate for the number of water molecules per lipid molecule, situated between the bilayers, $n_W - n'_W = 23$, cf. Sec. III, at 50 °C. This compares very well with our estimate of $n_W \simeq 22$ for DPPC-d_{62} at 49 °C (data not shown).

The relative changes in A with temperature can be measured directly by micropipette aspiration techniques applied to giant bilayer vesicles [48, 54]. The data for DMPC in Ref. [54] suggest that the relative change in area at the transition is $\Delta A/A_0 \simeq 0.2$ (A_0 is the area in the middle of the transition region), whereas our data for DMPC-$d-54$ imply that $\Delta A/A_0 \simeq 0.1$, i.e., a much smaller discontinuity. One should be careful with direct comparisons between data obtained for multilamellar systems and data obtained for giant bilayer vesicles. In the present case, it seems reasonable to compare the data obtained in the L_α phase. However, the amplitude and periodicity of the ripples in the $P_{\beta'}$ phase will probably be quite different, depending on, e.g., local forces between bilayers for the multilamellar system and lateral stress for the giant bilayer vesicles. This makes it more subtle to compare cross-sectional areas in the $P_{\beta'}$ phase.

Reference [54] gives results for the thermal area expansivity of DMPC, $C_T = (1/A)(\partial A/\partial T)$. By fitting A in Fig. 5(a) to smooth curves, separately below and above T_m, we can also obtain estimates for C_T for DMPC-d_{54}. The two sets of data are displayed in Table II. As expected from the considerations above, the agreement is good in the L_α phase, whereas the values obtained in the $P_{\beta'}$ phase are quite different.

Table II also displays our estimates for the isothermal area compressibility, i.e., $\tilde{\kappa}_A$ as calculated from Eq. (27), together with the values given in Ref. [54], where the compressibility modulus $(1/\kappa_A)$ was determined from micropipette aspiration techniques by detecting the linear response in relative area change, $\Delta A/A_0$, to the lateral pressure applied. In the L_α phase, κ_A from Ref. [54] is approximately 3.5 times larger than our estimate, $\tilde{\kappa}_A$. Taking into account that the systems are different, this implies that the Gaussian fluctuations, derived from our model, which are reflected in $\tilde{\kappa}_A$, represent the thermal fluctuations in the system to a reasonable extent in the L_α phase. The comparison is less favorable in the $P_{\beta'}$ phase, where the numbers differ by an order of magnitude. However, this was to be expected, since as discussed in Sec. V, the Gaussian fluctuations, derived from our model, in the $P_{\beta'}$ phase represent to a higher extent geometric fluctuations (i.e., the ripples) than real thermal fluctuations in the system.

VIII. DISCUSSION AND CONCLUSIONS

We have in this paper discussed small-angle neutron scattering from nonoriented, fully hydrated multilamellar lipid bilayers for temperatures near their main phase transition. We have argued that the scattering data are analyzed most adequately within paracrystalline theory in which the form and structure factors of the scattering intensity function remain coupled in the averaging procedure. By invoking a simple one-dimensional strip model of the lamellar stack, cf. Fig. 1, where each of the layers is assumed to exhibit Gaussian fluctuations, we have obtained structural and thermomechanic data from the system from a single type of experiment. The analysis not only leads to information on the lamellar repeat distance but also provides the thickness of the aqueous layers as well as the hydrophobic bilayer thickness. In addition, results for the molecular cross-sectional area as well as volumetric properties can be obtained. The results for the different quantities compare favorably with results obtained previously using other techniques, such as deuterium-NMR and micromechanics. Simple Gaussian fluctuations, derived for the structural data, lead to estimates for the response functions, e.g., the lateral area compressibility, which are comparable with experimentally obtained values, obtained in the L_α phase. The data for the repeat distance d and the hydrophilic aqueous layer thickness, d_A, in Figs. 4(a) and 4(c) demonstrate that the DMPC-d_{54} bilayers swell anomalously near the main phase transition [15] and exhibit a pronounced peak at the transition temperature. For both DMPC-d_{54} and DPPC-d_{62} the repeat distance increases very strongly in the fluid phase as the temperature is lowered towards the respective T_m. It is possible to analyze this behavior in terms of an apparent power-law singularity, $d(T) - d_0 \sim (T - T^*)^{-\psi}$ with $\psi = 1$, where T^* is the temperature of the apparent singularity (the pseudo-spinodal temperature) [29], and d_0 is the repeat distance in the fluid phase far from the phase transition. A similar effect has been observed earlier by Kirchner and Cevc [55]. The singularity corresponds to a critical unbinding transition [27, 28], which the system, however, never makes before the first-order chain-melting phase transition intervenes.

The anomalous swelling behavior observed can be interpreted in terms of a bilayer softening at the phase transition. The softening caused by the strong lateral density fluctuations leads to a thermal renormalization of the bilayer bending rigidity [15] and therefore stronger entropic undulation forces [27, 28], which in turn increase the bilayer separation. The reduction in bending rigidity in the transition region of fluid DMPC and DPPC bilayers has recently been observed directly by means of flicker-noise analysis [26]. It is noteworthy that the anomalous swelling is most pronounced for DMPC-d_{54}, which is consistent with the short-chain lipid being closer to a critical point [13, 14]. The general effect of undulation forces and repulsive interbilayer osmotic pressure as a means of controlling the swelling properties of multila-

mellar lipid systems has been observed in a number of other systems [5, 6, 56].

Our approach of analyzing the scattering data from multilamellar systems is conceptually different from both that of Nallet, Laversanne, and Roux [57] and Zhang, Suter, and Nagle [30] who decouple the form and structure factors. These authors describe the form factor by a model with some degree of internal structure, and for the structure factor they use a Hamiltonian approach based on the Caillé theory, cf. Eq. (4), for the scattering from a set of loosely coupled smectic layers [19]. Thus, whereas these authors have focused mainly on obtaining an accurate description of the structure factor, i.e., the fluctuations in the periodicity of the bilayers, our modeling aims more at obtaining an accurate knowledge of the structure of the individual bilayers, usually contained in the form factor.

Recently, Zhang *et al.* [31] have questioned the interpretation of the anomalous swelling behavior in terms of renormalization of bending rigidity as the transition is approached. As we already pointed out above, a pronounced lowering of the bending rigidity near the transition is an effect that has indeed been experimentally observed directly by Fernandez-Puente *et al.* [26] using flicker-noise analysis. Still, Zhang *et al.* [31] claim that their finding, from a shape analysis of the x-ray scattering from nonoriented multilamellar DMPC bilayers in terms of the Caillé theory, of a temperature-independent Caillé coefficient (which contains the bending modulus) invalidates our interpretation of the SANS data. However, the rough estimate made by Zhang *et al.* for the reduction in the bending rigidity necessary to induce the observed swelling effect close to the transition is in good agreement with the experimental results reported by Fernandez-Puente *et al.* From a thorough reading of the Zhang *et al.* paper it appears that these authors refer to ''anomalous swelling'' as the rapid variation of the repeat distance above the transition, whereas we proposed ''anomalous swelling'' to describe the peak behavior in the repeat distance at the transition [15]. Interestingly, the data for the repeat distance in the work by Zhang *et al.* display a small peak maximum near the transition, but this feature was not commented upon. A distinct peak behavior has been reported in other small-angle x-ray studies on DMPC multilamellar bilayers [45, 46]. It is clear from the data from the present work presented in Fig. 4 that both the hydrophobic bilayer thickness as well as the hydrophilic thickness (including the water layer) change rather strongly in the transition region. Moreover, as seen from Fig. 4(b), the present results for the hydrophobic thickness are consistent with the NMR data in the fluid phase.

The resolution of the x-ray data published by Zhang *et al.* [31] for DMPC is much better than what we can obtain from SANS measurements. As argued in Sec. II of the present paper we do not find it justified to interpret our scattering data in terms of a simple harmonic theory (the Caillé theory) as was done by Zhang *et al.* The harmonic theory is expected to break down when strong fluctuations prevail, which is precisely the case close to the phase transition. A main finding of the present SANS work is that the bilayer is close to a critical unbinding transition. This statement is independent of our actual model since it only uses the data for the repeat distance, which can be obtained to a very good approximation from the positions of the lowest-order Bragg peak [15]. We are therefore far from the regime controlled by Gaussian modes where the simple harmonic theory applies.

The results of the analysis performed by Zhang *et al.* [31] based on the Caillé theory in fact indicates a breakdown of the harmonic theory near the transition since the values found for the Caillé parameter η_n, for the first- and second-order peaks are $\eta_1 = 0.19$ and $\eta_2 = 0.41$ with a ratio of about 0.5, which is far from the value 0.25 predicted by the harmonic theory [cf. Eq. (6)]. Hence we contend that the interpretation of the detailed line-shape analysis performed by Zhang *et al.* does not hold in the temperature region that we are concerned with in the present paper.

In closing, it should be emphasized that the approach presented in the present paper to analyze data from SANS measurements on fully hydrated multilamellar phospholipid bilayers represents one of the first quantitative attempts to gain insight into the coupled fluctuation effects that prevail in fully hydrated multilamellar phospholipid bilayers close to the main phase transition. The approach can readily be extended to study the effects of small amounts of solutes, e.g., cholesterol, incorporated into the bilayer.

ACKNOWLEDGMENTS

This work was supported by the Danish Natural Science Research Council and the Danish Technical Research Council. Illuminating discussions with Steven H. White, Evan Evans, and John F. Nagle are gratefully acknowledged. O.G.M. is an Associate Fellow of the Canadian Institute for Advanced Research.

[1] M. Bloom, E. Evans, and O. G. Mouritsen, Quart. Rev. Biophys. **24**, 293 (1991).

[2] *Functional Dynamics of Lipids in Biomembranes*, edited by P. K. J. Kinnunen and O. G. Mouritsen special issue of Chem. Phys. Lipids **73**, 1 (1994).

[3] For a recent review of fluid-lipid-bilayer structure determination by x-ray and neutron scattering, see S. H. White and M. C. Wiener, in *Permeability and Stability of Lipid Bilayers*, edited by E. A. Disalvo and S. A. Simon (CRC Press, Boca Raton, FL, 1994), p. 89.

[4] G. Büldt, H. U. Gally, J. Seelig, and G. Zaccai, J. Mol. Biol. **134**, 673 (1979).

[5] T. J. McIntosh, and S.A. Simon, Annu. Rev. Biophys. Biomol. Struct. **23**, 27 (1994).

[6] V. A. Parsegian and R. P. Rand, in *Handbook of Biophysics*, edited by R. Lipowski and E. Sackmann (Springer-Verlag, Berlin, 1995), p. 643.

[7] J. F. Nagle, Annu. Rev. Phys. Chem. **31**, 157 (1980).

[8] O. G. Mouritsen, Chem. Phys. Lipids **57**, 178 (1991).

[9] J. F. Nagle and D. A. Wilkinson, Biophys. J. **23**, 159 (1978).

[10] M. C. Wiener, S. Tristram-Nagle, D. A. Wilkinson, L. E. Campbell, and J. F. Nagle, Biochim. Biophys. Acta **938**, 135 (1988).
[11] Abbreviations used: DMPC, dimyristoyl phosphatidylcholine; DPPC, dipalmitoyl phosphatidylcholine; with saturated fatty-acid chain lengths corresponding to 14 and 16 carbon atoms, respectively.
[12] J. Risbo, M. M. Sperotto, and O. G. Mouritsen, J. Chem. Phys. **103**, 3643 (1995).
[13] M. R. Morrow, J. P. Whitehead, and D. Lu, Biophys. J. **63**, 18 (1992).
[14] J. H. Ipsen, K. Jørgensen, and O. G. Mouritsen, Biophys. J. **58**, 1099 (1990).
[15] T. Hønger, K. Mortensen, J. H. Ipsen, J. Lemmich, R. Bauer, and O. G. Mouritsen, Phys. Rev. Lett. **72**, 3911 (1994).
[16] J. Lemmich, J. H. Ipsen, T. Hønger, K. Jørgensen, O. G. Mouritsen, K. Mortensen, and R. Bauer, Mod. Phys. Lett. B **8**, 1803 (1994).
[17] R. Hosemann and S. N. Bagchi, *Direct Analysis of Diffraction by Matter* (North-Holland, Amsterdam, 1962), pp. 216ff, 302ff.
[18] R. Hosemann and S. N. Bagchi, *Direct Analysis of Diffraction by Matter* (North-Holland, Amsterdam, 1962), p. 408ff.
[19] A. Caillé, C. R. Acad. Sci. Ser. B **274**, 891 (1972).
[20] A. Guinier, *X-Ray Diffraction* (Freemann, San Francisco, 1963), pp. 51–53.
[21] W. Helfrich, Z. Naturforsch. **28c**, 693 (1973).
[22] W. Helfrich, Z. Naturforsch. **33a**, 305 (1978).
[23] C. R. Safinya, D. Roux, G. S. Smith, S. K. Sinha, P. Dimon, N. A. Clark, and A.-M. Bellocq, Phys. Rev. Lett. **57**, 2718 (1986).
[24] J. Als-Nielsen, J. D. Lister, R. J. Birgeneau, M. Kaplan, C. R. Safinya, A. Lindegaard-Andersen, and S. Mathiesen, Phys. Rev. B **22**, 312 (1980).
[25] G. Porte, J. Marignan, P. Bassereau, and R. May, Europhys. Lett. **7**, 713 (1988).
[26] L. Fernandez-Puente, I. Bivas, M. D. Mitov, and P. Méléard, Europhys. Lett. **28**, 181 (1994).
[27] R. Lipowsky and S. Leibler, Phys. Rev. Lett. **56**, 2541 (1986).
[28] R. Lipowsky, Europhys. Lett. **7**, 255 (1988).
[29] J. Lemmich, K. Mortensen, J. H. Ipsen, T. Hønger, R. Bauer, and O. G. Mouritsen, Phys. Rev. Lett. **75**, 3958 (1995).
[30] R. Zhang, R. M. Suter, and J. F. Nagle, Phys. Rev. E **50**, 5047 (1994).
[31] R. Zhang, W. Sun, S. Tristram-Nagle, L. Headrick, R. M. Suter, and J. F. Nagle, Phys. Rev. Lett. **74**, 2832 (1995).
[32] J. Lemmich, K. Mortensen, J. H. Ipsen, T. Hønger, R. Bauer, and O. G. Mouritsen (unpublished).
[33] T. R. Welburry, Rep. Prog. Phys. **48**, 1543 (1985).
[34] V. F. Sears, Methods Exp. Phys. **23A**, 521 (1986).
[35] K. Müller, in *Small Angle X-ray Scattering*, edited by O. Glatter and O. Kratky (Academic, London, 1982), p. 215.
[36] R. Brämer, Kolloid Z. Polym. **250**, 1034 (1972).
[37] B. Crist, J. Polym. Sci. Polym. Phys. Ed. **11**, 635 (1973).
[38] R. Zhang, S. Tristram-Nagle, W. Sun, R. L. Headrick, T. C. Irving, R. M. Suter, and J. F. Nagle, Biophys. J. **70**, 349 (1996).
[39] J. F. Nagle and M. C. Wiener, Biochim. Biophys. Acta **942**, 1 (1988)
[40] A. Tardieu, V. Luzatti, and F. C. Reman, Biophys. J. **75**, 711 (1973).
[41] D. C. Wack and W. W. Webb, Phys. Rev. A **40**, 2712 (1989).
[42] M. J. Janiak, D. M. Small, and G. G. Shipley, J. Biol. Chem. **254**, 6068 (1979).
[43] K. Mortensen, W. Pfeiffer, E. Sackmann, and W. Knoll, Biochim. Biophys. Acta **945**, 221 (1988).
[44] S. Matuoka, S. Kato, M Akiyama, Y. Amemiya, and I. Hatta, Biochim. Biophys. Acta **1028**, 103 (1990).
[45] S. Matuoka, S. Kato, and I. Hatta, Biophys. J. **67**, 728 (1994).
[46] S. Korremann, M.Sc. Thesis, University of Roskilde, Denmark, 1995.
[47] J. S. Pedersen, D. Posselt, and K. Mortensen, J. Appl. Cryst. **23**, 321 (1990).
[48] E. Evans and R. Kwok, Biochemistry **21**, 4874 (1982).
[49] Y. Inoko and T. Mitsui, J. Phys. Soc. Jpn. **44**, 1918 (1978).
[50] A. Seelig and J. Seelig, Biochemistry **13**, 4839 (1974).
[51] H. Schindler and J. Seelig, Biochemistry **14**, 2283 (1975).
[52] J. H. Ipsen, O. G. Mouritsen, and M. Bloom, Biophys. J. **57**, 405 (1990).
[53] J. F. Nagle, Biophys. J. **64**, 1476 (1993).
[54] D. Needham and E. Evans, Biochemistry **27**, 8261 (1988).
[55] S. Kirchner and G. Cevc, Europhys. Lett. **23**, 229 (1993).
[56] S. A. Simon, S. Advani, and T. J. McIntosh, Biophys. J. **69**, 1473 (1995).
[57] F. Nallet, R. Laversanne, and D. Roux, J. Phys. (France) II **3**, 487 (1993).